2022

Assessment of Combined Modality Therapy for Non-Small-Cell Lung Carcinoma: A Simulation Study Concerning Concurrent Chemo-Brachytherapy

Hadi Rezaei

Hesameddin Mostaghimi
Old Dominion University, hmost001@odu.edu

Ali Reza Mehdizadeh

Original Publication Citation

Rezaei, H., Mostaghimi, H., & Mehdizadeh, A. R. (2022). Assessment of combined modality therapy for non-small-cell lung carcinoma: A simulation study concerning concurrent chemo-brachytherapy. *Journal of Cancer Research and Therapeutics*, *18*(4), 946-952.

Original Article

Assessment of combined modality therapy for non-small-cell lung carcinoma: A simulation study concerning concurrent chemo-brachytherapy

Hadi Rezaei[1], Hesameddin Mostaghimi[2], Ali Reza Mehdizadeh[3]

[1]Department of Medical Physics and Biomedical Engineering, School of Medicine, Tehran University of Medical Sciences, Tehran, Iran, [2]Biomedical Engineering Institute, Frank Batten College of Engineering and Technology, Old Dominion University, Norfolk, VA, USA, [3]Department of Biomedical Physics and Engineering, School of Medicine, Shiraz University of Medical Sciences, Shiraz, Iran

For correspondence: Hesameddin Mostaghimi, PhD Student in Biomedical Engineering-Biomedical Engineering Institute/ Frank Batten College of Engineering & Technology- Old Dominion University, Norfolk, VA, USA. E-mail: hmost001@odu.edu

ABSTRACT

Although surgery is the treatment of choice for early-stage non-small-cell lung carcinoma, almost two-thirds of patients do not have acceptable pulmonary function for extensive surgeries. The alternative approach for this large group of patients is sublobar resection along with low-dose-rate (LDR) brachytherapy (BT). However, patients with resected lungs have a high risk of recurrence and are often treated with platinum-based (Pt-based) chemotherapy (CT). In this study, we aimed to evaluate the absorbed doses of lung and other thoracic organs, considering concurrent chemo-BT with LDR sources in two modalities: conventional vs. unconventional Pt-based CT. We used the MCNPX code for simulations and to obtain the lung absorbed dose, dose enhancement factor (DEF), and Pt threshold concentration for the abovementioned modalities. Our results indicate that DEF correlates directly with Pt concentration at prescription point and is inversely correlated with depth. Dose enhancement for conventional CT concurrent with BT is <2%, while it is >2% in case of unconventional Pt-based CT wherein the Pt concentration exceeds 0.2 mg/g lung tissue. Also, the absorbed dose of healthy thoracic organs decreased by 2–11% in the latter approach. In conclusion, the concurrent chemo-BT in the lung environment could enhance the therapeutic doses merely by using unconventional CT methods, while lung Pt accumulation exceeds 0.2 mg/g.

KEY WORDS: Combined modality therapy, concurrent chemo-brachytherapy, low-dose-rate brachytherapy, non-small-cell lung carcinoma, platinum-based chemotherapy

INTRODUCTION

Although lung cancer constitutes about 15% of all diagnosed cancers, it leads to the highest mortality rate among both male and female patients.[1] With 80–85% prevalence, non-small-cell lung carcinoma (NSCLC) is the most common lung cancer.[2] The standard treatment for early-stage NSCLC is lobectomy or pneumonectomy; nonetheless, about two-thirds of patients do not have acceptable respiratory conditions to undergo such extensive surgeries.[3] Furthermore, the 5-year survival rate is less than 50% following lobectomy or pneumonectomy.[4] An alternative approach for these patients is to remove a smaller part of the lung by wedge resection plus low-dose-rate (LDR) permanent implant brachytherapy (BT), which has shown promising local control and survival rates.[5,6] In this technique, an implant is created during surgery by weaving strands of LDR BT seeds into a vicryl mesh which is then sutured over the resection staple line with the goal of delivering 100–120 Gy to the prescription point.[7,8]

Santos *et al*.[9] reported 18.6% recurrence for surgery alone versus 2% for wedge resection plus ^{125}I seed BT. Peters *et al*.[10] reported about 50% recurrence in less than 1 year after complete resection (surgery alone) for patients in stages IB and II. Therefore, for high-risk patients in early stages, adjuvant chemotherapy (CT) with platinum (Pt)-based CT drugs is recommended which can be concurrently administered with BT.[11,12] On the other hand, Van Dyk indicated that only a small increase in the lung absorbed dose can significantly increase the probability of radiation pneumonitis.[13] So, it is reasonable to assess dose changes in the lung and

Cite this article as: Rezaei H, Mostaghimi H, Mehdizadeh AR. Assessment of combined modality therapy for non-small-cell lung carcinoma: A simulation study concerning concurrent chemo-brachytherapy. J Can Res Ther 2022;18:946-52.

Submitted: 25-May-2020
Revised: 16-Jul-2020
Accepted: 27-Apr-2022
Published: 22-Sep-2022

Access this article online
Website: www.cancerjournal.net
DOI: 10.4103/jcrt.JCRT_689_20
Quick Response Code:

other thoracic tissues caused by the concurrent use of LDR BT with Pt-based CT considering the following points:

1. Some studies have reported that lung *Pt concentration* following conventional systemic Pt-based CT is in the range of 1–10 μg/g lung tissue, independent from the number of CT cycles and time since last CT.[14-16] Therefore, the first question is whether conventional systemic Pt-based CT concurrent with LDR permanent implant BT may significantly change the lung absorbed dose.
2. Since the antineoplastic effects of Pt-based CT drugs are due to Pt accumulation in the target tissue,[15,17] several prospective Pt-based complexes and novel methods have been innovated to maximize target *Pt concentration*.[18-41] Thus, the second question is whether the novel drugs and methods, which we call unconventional Pt-based CT, can significantly influence the lung absorbed dose in a concurrent chemo-BT with LDR sources. If so, what is the Pt threshold concentration which leads to >2% increase in the lung absorbed dose, and how will the dose to healthy thoracic organs be affected?

Prior to this study, we had also performed related investigations in a multistage project[16,42,43] which their results are used in our simulations.

In this study, we used the MCNPX code to simulate the thorax phantom, including the lungs, heart, vertebral column, and ribs, and tested different configurations of ^{125}I and ^{103}Pd seeds as well as various *Pt concentrations* (1–10 μg/g for conventional vs. 50–500 μg/g for unconventional CT). In the end, we calculated the lung absorbed dose, dose enhancement factor (*DEF*), dose profiles, and Pt threshold concentration, which led to significant dose enhancement.

MATERIALS AND METHODS

Pt concentration

There is limited data on the Pt content of human lungs following Pt-based CT. Stewart *et al.*[14] reported postmortem human tissue *Pt concentration* after cisplatin CT, obtained from the autopsy samples of patients who had received cisplatin. *Pt concentration* was highest in the liver, prostate, and kidney and lowest in some tissues including the lung (0–3 μg/g). Another study conducted by Kim[15] reported lung *Pt concentration* in the range of 0–8 μg/g following cisplatin and carboplatin CT. We also measured *Pt concentration* in the lung tissue and tumor by inductively coupled plasma spectroscopy in our previous study.[16] Our results showed that the *Pt accumulation* in the lung was in the range of 0.17–7.23 μg/g (mean 3.12). As a result, we considered 1–10 μg/g *Pt concentration* for conventional systemic Pt-based CT in our simulations.

On the other hand, novel methods like regional CT, intraarterial CT/isolated lung perfusion, can increase the *Pt concentration* in the target tissue through the artery directly linked to the lung. Also, new multinuclear Pt-based drugs (e.g., bisplatinum and BBR3464) are reported to increase the lung *Pt accumulation* because of the higher *Pt concentration* in their nuclei. So, considering these novel methods and drugs which lead to 5–100 times higher *Pt accumulation*,[38-41] we used 50–1000 μg/g Pt for unconventional CT approach in our simulations (5–100 times higher than 10 μg/g).

Since the pharmacokinetics and distribution of Pt-based drugs depend on different variables and are not yet clear following CT, we considered a homogeneous Pt distribution in our simulations.

Lung mesh implants

Lung mesh seed implants can be used to cover a target area of about 50 cm^2.[5,9,44] We have previously evaluated different configurations of ^{125}I and ^{103}Pd seeds in lung implantation.[43] These implants were selected based on other studies done by Chen *et al.*,[44] Johnson *et al.*,[45] and Sutherland *et al.*[46] Ten seeds were put in each row with a 1 cm center-to-center distance though with varying row spacing due to the different number of rows. Row spacing was 0.8, 1, 1.3, and 1.5 cm for 60, 50, 40(I), and 40(II) seed configurations, respectively. Different arrangements were set up with the same total source strength (air-kerma strength) to deliver a specific dose (100 Gy) to the prescription point. Table 1 shows 4 mesh configurations and their relevant source strength (per seed) modified for lung heterogeneity by the present authors in.[43] Figure 1a demonstrates configuration II (40 seeds) versus IV (60 seeds) in a 5 × 10 cm^2 vicryl mesh.

Radiation transport

The MCNPX transport code version 2.6.0 (Los Alamos National Laboratory, New Mexico, USA) was used to simulate the thorax phantom including lungs with various *Pt concentrations* (0–0.5 mg/g) and four configurations of the ^{125}I and ^{103}Pd seeds to calculate the lung *absorbed dose* in various cases. Considering the energy range of ^{125}I and ^{103}Pd seeds and the detector size (1 mm^3 cubic voxel), electron equilibrium exists and the collision kerma is a good estimation of the *absorbed dose*. The F6 track-length estimator was used to obtain dose per history and was converted to total *absorbed dose* as follows[46]:

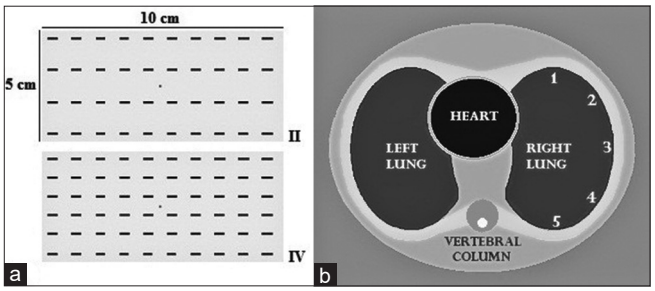

Figure 1: (a) Configuration II (40 seeds) versus configuration IV (60 seeds) on a 5 × 10 cm^2 vicryl mesh. (b) Thorax phantom cross-section, including the lungs, heart, ribs, and vertebral column. Numbers 1–5 indicate the 5 mesh positions in the right lung

$$\textit{Total absorbed dose (cGy)} = \textit{MC output (MeV/g per photon)} \times 1/S_k\,(\textit{cm}^2.\textit{MeV/g per photon})^{-1} \times S_k\,(U) \times \tau\,(h) \quad \textbf{(1)}$$

where MC output is the F6 tally output (dose per history), s_k is air-kerma strength per history obtained from the MC calculations, S_k is the initial air-kerma strength in the treatment, and τ is the source's mean lifetime (treatment time). The calculation of air-kerma strength per history (s_k) for a particular seed is described by Taylor *et al*.[47] In total, 1.5×10^9 photon histories were considered to achieve the maximum accuracy (max error 1%). The default cross-sections of the MCNPX were used for various *Pt concentrations*, and the particle interactions were treated by (ENDF)/B library. The cut-off energies for photons and electrons were set to 5 and 10 keV, respectively.

Thorax phantom

By using quadratic equations, we simulated a thorax phantom including lungs, heart, ribs, and vertebral column with their constituent compositions and densities. We simulated the thorax as an elliptical cylinder with a 20 × 30 cm^2 cross-section, including two other elliptical cylinders as lungs with cross-sections of 12 × 16 cm^2. The heart was simulated as an oval with 3, 4, and 5.5 cm diameters so that two-thirds of it lied to the left of the midline. A part of the right lung with a 50 cm^2 cross-section was removed as the resected part and the seed mesh was placed on it. The composition and mass densities of the thoracic organs are mentioned in Table 2.[48,49] Figure 1b illustrates the cross-section of the simulated thorax phantom and 5 mesh positions in the right lung. In each program, a particular setup in a specific position was used.

^{125}I Seed (Amersham, model 6711)

The ^{125}I source (model 6711) was simulated based on an actual three-dimensional source by MC simulation and benchmarked, in our previous study.[42] A titanium capsule of density 4.54 g/cm^3 filled with argon gas (ρ = 1.784 g/cm^3), contained a silver cylindrical marker of density 10.5 g/cm^3, with 2.8 mm length and 0.254 mm radius, was covered with a 2-μm Br_5I_2 layer (ρ = 6.245 g/cm^3). The source's effective length was 2.8 mm, and its end was curved by 0.045 mm at 45° angles. The average energy, half-life, and mean life-time of the ^{125}I source are 28.37 keV, 59.4, and 85.7 days, respectively.

^{103}Pd Seed (Theragenics, model 200)

The ^{103}Pd seed (Theragenics, model 200) was simulated based on an actual three-dimensional source and benchmarked, in our previous studies.[43,50] This seed contained two cylindrical graphite rods of density 2.22 g/cm^3, 0.56 mm in diameter, and 0.890 mm in length, which were coated with a thin layer of radioactive Pd of density 12.03 g/cm^3 and 2.2 μm thick. The graphite cylinders were separated by a lead marker of density 11.4 g/cm^3, 0.5 mm in diameter, and 1.09 mm in length. This compound was enclosed in a cylindrical titanium capsule of density 4.51 g/cm^3, 0.826 mm in external diameter, and 0.056 mm thick. The total length of this source was 4.5 mm with an effective length of 4.23 mm. The average energy, half-life, and mean life-time of the ^{103}Pd source are 20.74 keV, 16.99, and 24.5 days, respectively.

AAPM task group No. 43 (TG-43) parameters

The dosimetry parameters of the ^{125}I and ^{103}Pd sources were calculated and benchmarked in our previous studies, based on the AAPM TG-43U1 protocol. According to this protocol, the dosimetry parameters of BT sources are governed by the following equation:

$$\dot{D}(r,\theta) = S_k \Lambda\,[G(r,\theta)/G(r_0,\theta_0)]\,g(r)\,F(r,\theta) \quad \textbf{(2)}$$

where $\dot{D}(r, \theta)$ and S_k are dose rate and air-kerma strength of

Table 1: Initial air-Kerma (source) strength per seed (U/seed) per prescription dose (100 Gy) for various configurations of ^{125}I and ^{103}Pd brachytherapy sources. Source strengths are modified for lung heterogeneity by the present authors in ref. [43]

Various Mesh Arrangements				Modified Source Strength* (U/prescription dose)	
Configuration	No. of Seeds	Rows×Columns	Row Spacing (cm)	^{125}I	^{103}Pd
I	40	4×10	1.5	0.61	2.88
II	40	4×10	1.3	0.56	2.53
III	50	5×10	1.0	0.41	1.90
IV	60	6×10	0.8	0.33	1.58

*Based on the AAPM TG-43 protocol, the dosimetry parameters of low-dose-rate brachytherapy sources are calculated in a homogeneous water phantom. According to significant differences between the homogeneous water and the inhomogeneous lung, we have previously modified the ^{125}I and ^{103}Pd source strengths at the prescription point for lung heterogeneity[43]

Table 2: Elemental composition and mass densities of thoracic tissues used in our simulations[48,49]

Organs	Elemental Composition (mass %)					ρ g/cm^3
	H	C	N	O	Elements with Z >8	
Soft tissue	10.2	11.2	3.0	74.5	Na (0.1), P (0.2), S (0.3), Cl (0.1), K (0.4)	1.05
Lung	10.3	10.5	3.1	74.9	Na (0.2), P (0.2), S (0.3), Cl (0.3), K (0.2)	0.26
Heart	10.3	12.1	3.2	73.4	Na (0.1), P (0.1), S (0.2), Cl (0.3), K (0.2), Fe (0.1)	1.06
Ribs	6.4	26.3	3.9	43.6	Na (0.1), Mg (0.1), P (6.0), S (0.3), Cl (0.1), K (0.1), Ca (13.1)	1.41
Vertebra	3.4	15.5	4.2	43.5	Na (0.1), Mg (0.2), P (10.3), S (0.3), Ca (22.5)	1.92
Water	11.22	0.0	0.0	88.78		0.998
Air (TG-43)	0.07	0.01	75.03	23.61	Ar ($\bar{1}.27$)	0.0012

the source, respectively, Λ is the dose rate constant at the reference point (1 cm, π/2), and G (r, θ), g (r), and F (r, θ) are geometry, radial dose, and anisotropy functions, respectively. In our previous studies, these parameters were also compared with those from other studies, and in this study, the previously validated sources (programs) were used.

Absorbed dose and dose enhancement factor

The purpose of putting mesh with LDR seeds is to deliver 100 Gy dose to the prescription point. To obtain depth dose with high resolution, 50 cubic detectors with 1 mm^3 volume were considered on the central axis at a 5-cm depth. We also used 1 mm^3 detectors at the center of the lungs, heart, and vertebral column. Considering Equation (1) and the F6 tally output, *absorbed dose* was calculated in the lungs and healthy thoracic tissues for 0–0.5 mg/g *Pt concentrations*. The *DEF* in the lungs and other thoracic tissues due to Pt presence were calculated as follows:

$$DEF = D_{Pt}/D_0 \quad (3)$$

where D_{Pt} and D_0 are the *absorbed dose* at a particular detector with and without Pt, respectively.

RESULTS

Following the simulation and validation of the ^{125}I and ^{103}Pd sources, 4 mesh configurations [Table 1] were simulated on the resected part of the lung (five positions mentioned in Figure 1b) and the lung *absorbed dose* was calculated for various *Pt concentrations* (0–0.5 mg/g lung tissue) up to 5 cm in depth. In addition, *DEF* per depth, per *Pt concentration*, and at the center of healthy organs were also obtained.

Figure 2a and 2b illustrate lung depth dose for configurations I–IV up to 1 cm (*PDD* ≈ 70%) for the ^{125}I and ^{103}Pd sources, respectively. These figures show the comparison of the mentioned arrangements in the case that no CT was administered. The relative standard deviation (*%RSD*) of configurations I–III with respect to the 50-seed arrangement (III) is presented in Table 3 for both sources. Table 4 indicates the lung *absorbed dose* per depth in the case of concurrent Pt-based CT and LDR BT with the 50-seed configuration up to 5 cm (*PDD* ≈ 10%) in depth. Both conventional and unconventional CT were considered and are shown in the table. *DEFs* per *Pt concentration* in the lung are indicated in Figure 3a and 3b for the ^{125}I and ^{103}Pd sources, respectively. These data are presented for the prescription point (d = 0.5 cm) and some further depths. Table 5 demonstrates the *DEF* at the center of the right and left lungs, heart, and vertebral column in the case of concurrent unconventional Pt-based CT and mesh BT for 0.2 and 0.5 mg/g *Pt concentrations*.

DISCUSSION

Figure 2 indicates lung depth dose for 40-, 50-, and 60-seed arrangements up to 1 cm in depth. As it is shown, the prescription dose at d = 0.5 cm is equal (100 Gy) for all seed configurations according to the same overall source (air-kerma) strength. Total source strength for each arrangement was obtained by multiplying seed number by the source's initial air-kerma strength (U/seed), mentioned in Table 1. At other depths, minor differences were observed between different cases (I– IV). Table 3 shows relative standard deviation (%RSD) for the 40- and 60-seed setups with respect to the 50-seed arrangement for both sources. As expected, %RSD at d = 0.5 cm is 0. %RSD is highest at the initial distances (prescription area: 0.1–0.5 cm), 10–12% for the

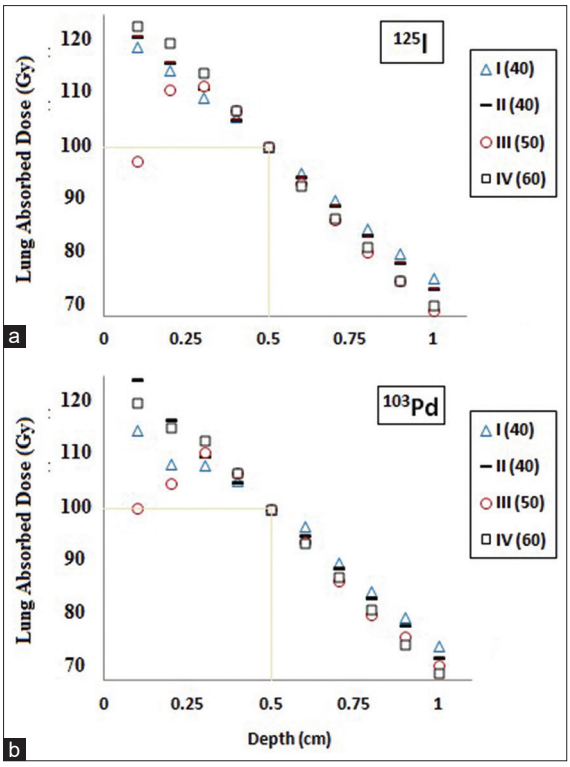

Figure 2: Lung absorbed dose per depth for 40-, 50-, and 60-seed configurations of the (a) 125I and (b) 103Pd sources mentioned in Table 1

Table 3: Relative standard deviation (%RSD) of mesh configurations I, II, and IV with respect to 50-seed arrangement (III) in lung tissue (without chemotherapy) for ^{125}I and ^{103}Pd brachytherapy sources

Depth (cm)	^{125}I			^{103}Pd		
	$I_{(III)}$	$II_{(III)}$	$IV_{(III)}$	$I_{(III)}$	$II_{(III)}$	$IV_{(III)}$
0.1	10.03	10.85	11.66	6.97	10.71	9.09
0.2	1.77	2.20	3.89	1.87	5.40	4.97
0.3	1.35	0.44	0.88	1.37	0.45	0.89
0.4	0.47	0.94	0.01	0.47	0.94	0.02
0.5*	0	0	0	0	0	0
0.6	1.06	0.64	0.21	1.51	0.58	0.21
0.7	1.98	1.42	0.05	1.98	1.42	0.51
0.8	2.41	1.95	0.49	2.60	1.95	0.55
0.9	2.23	2.15	0.13	2.30	1.29	0.99
1.0	2.19	2.02	0.86	2.40	1.04	1.06

*Equal prescription dose (100 Gy) due to the same overall source strength

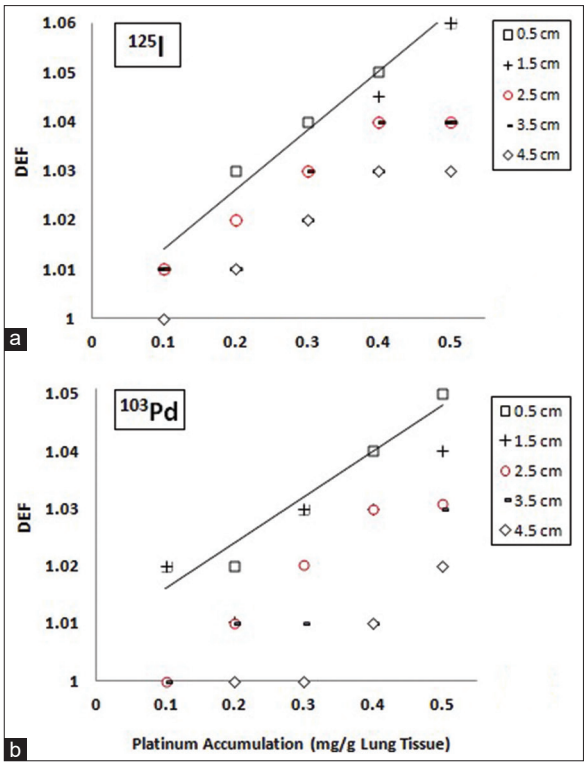

Figure 3: Dose enhancement factor (DEF) per lung platinum accumulation at the prescription point (d = 0.5 cm) and some further depths for the (a) 125I and (b) 103Pd sources. The trend line shows a direct correlation between DEF and platinum concentration at the prescription point

^{125}I source and 11–16% for the ^{103}Pd source at $d = 0.1$ cm. In this area, the lung *absorbed dose* for all cases is higher than the prescription dose by 100–120 Gy [Figure 2]. However, at further depths, the RSD% decreased beneath 2% for all cases. Since we evaluate the *absorbed dose* and the *DEFs* beyond the prescription point ($d > 0.5$ cm) and most of the %RSDs were minor, the 50-seed arrangement data is adequate. For other mesh configurations, the same trend and similar results were observed.

Table 4 presents the lung *absorbed dose* up to 5 cm in depth in the case of concurrent Pt-based CT and LDR BT with various *Pt concentrations* (0–500 μg/g). As explained in the section "2.1 Pt Concentration," 1–10 and 50–500 μg/g Pt were considered for conventional[14-16] and unconventional[38-41] Pt-based CT, respectively. Since the calculation accuracy was 1% in our simulations and only >2% differences were considered significant (based on the ICRU standard), the dose changes were not meaningful (<1%) in the case of conventional CT (1–10 μg/g). Therefore, no significant changes were observed for the concurrent chemo-BT with conventional Pt-based CT. However, in cases where lung *Pt accumulation* exceeded 200 μg/g, the dose increase surpassed 2% for both seed arrangements. As shown in Table 4, the *absorbed dose* (and consequently the *DEF*) correlates inversely with depth.

Table 4: Lung absorbed dose per depth in the case of concurrent platinum-based chemotherapy and low-dose-rate mesh brachytherapy with 50-seed configuration (III)

^{125}I (Amersham 6711)										
Depth (cm)	Platinum Concentration (μg/g Lung Tissue)									
	No CT	Conventional Systemic CT			Unconventional CT					
	0	1	5	10	50	100	200	300	400	500
0.1	97.3	97.5	97.5	97.7	98.0	98.6	99.8	101	102	104
0.5*	100†	100	99.9	100	101	101	103	104	105	106
1.0	69.6	69.6	69.7	69.9	70.0	70.4	71.3	72.1	73.0	73.7
1.5	51.2	51.3	51.4	51.7	51.5	51.7	52.3	52.8	53.5	54.1
2.0	39.3	39.4	39.6	39.5	39.3	39.5	39.9	40.3	40.7	41.0
2.5	30.5	30.5	30.4	30.3	30.6	30.7	31.2	31.5	31.7	31.9
3.0	24.1	24.0	24.0	24.1	24.2	24.3	24.5	24.7	24.8	25.1
3.5	19.6	19.5	19.6	19.7	19.7	19.7	19.8	20.1	20.3	20.3
4.0	16.0	15.9	15.9	16.0	16.1	16.2	16.3	16.3	16.5	16.7
4.5	13.2	13.2	13.2	13.2	13.2	13.2	13.3	13.4	13.6	13.5
5.0	11.1	11.0	11.0	10.9	11.1	11.1	11.1	11.2	11.3	11.3
^{103}Pd (Theragenics 200)										
0.1	100	101	101	101	101	102	102	103	105	105
0.5*	100†	101	101	101	101	102	102	103	104	104
1.0	68.7	68.9	68.9	69.0	69.1	69.4	70.0	70.2	70.8	70.8
1.5	49.6	50.0	50.0	50.0	49.8	50.4	50.3	50.2	50.8	50.3
2.0	35.3	35.6	35.6	35.6	35.5	36.0	35.9	36.0	36.3	36.2
2.5	27.1	27.3	27.3	27.3	27.1	27.3	27.2	27.1	27.4	27.3
3.0	20.7	20.8	20.8	20.8	20.8	20.8	20.6	20.6	20.6	20.5
3.5	16.7	16.8	16.8	16.9	16.7	16.6	16.5	16.5	16.5	16.7
4.0	13.0	13.0	13.0	13.0	13.0	12.9	13.0	12.6	12.3	12.5
4.5	10.2	10.3	10.3	10.3	10.1	10.1	10.2	10.2	10.1	10.1
5.0	8.23	8.11	8.11	8.09	8.22	8.22	8.05	7.99	7.99	7.96

*Prescription Point=0.5 cm from seeds mesh† Prescription Dose=100 Gy (through permanent implantation)

Table 5: Dose enhancement factors (DEFs) at the center of the heart, vertebral column, left and right lungs in the case of concurrent Pt-based chemotherapy and mesh brachytherapy for 0.2 and 0.5 mg/g lung platinum accumulation and 5 mesh positions (according to Figure 1b)

^{125}I (Amersham 6711)										
Thorax Organs	0.2 (mg/g) Pt					0.5 (mg/g) Pt				
	1	2	3	4	5	1	2	3	4	5
Right Lung	0.98	0.99	0.99	0.98	0.97	1.00	1.01	1.02	1.01	0.99
Left Lung	0.93	0.94	0.95	0.94	0.96	0.90	0.92	0.93	0.93	0.95
Heart	1.00	0.99	0.98	0.97	0.95	0.99	0.97	0.97	0.95	0.93
Vertebral Column	0.95	0.97	0.97	0.99	1.00	0.91	0.93	0.95	0.98	0.99
^{103}Pd (Theragenics 200)										
Right Lung	0.96	0.97	0.98	0.97	0.97	0.98	1.00	1.01	1.01	0.98
Left Lung	0.93	0.94	0.94	0.95	0.96	0.90	0.92	0.91	0.93	0.94
Heart	0.99	0.98	0.98	0.95	0.93	0.97	0.96	0.97	0.94	0.90
Vertebral Column	0.93	0.96	0.97	0.98	0.99	0.89	0.92	0.94	0.97	0.97

*DEFs for different mesh configurations are similar (RD<1%) due to same total source strength

Figure 3 demonstrates *DEF* per lung *Pt accumulation* (0.1–0.5 mg/g) at the prescription point and some further depths. Figure 3a and 3b are relevant to the ^{125}I and ^{103}Pd sources, respectively. The trend line shows a direct correlation between *DEF* and *Pt concentration*. In addition, the *DEF*

gradient for ^{125}I is slightly steeper than that for ^{103}Pd. For both sources, the *DEF* at the prescription point passed 1.02 when *Pt concentration* exceeded 0.2 mg/g. Although this increasing trend was observed at other distances, the *DEF* at further depths or lower concentrations is ≤1.

Table 5 indicates the *DEF* at the center of healthy thoracic organs (lungs, heart, and vertebral column) in the cases of concurrent chemo-BT with 0.2 and 0.5 mg/g *Pt concentrations* (unconventional CT). These results were obtained for the five different mesh positions shown in Figure 1b. In general, the DEF at healthy tissue was less than 1, which shows the reduction of *absorbed dose* by 2–11%, due to increased photoelectric absorption caused by high Z Pt. Moreover, the *absorbed dose* and the DEF at healthy thoracic organs decreased with an increase in lung *Pt accumulation*. Since the right lung contained the seed mesh, the *DEFs* at its center are higher than 1 due to increased photoelectric absorption adjacent to the prescription area. At further distances, the dose and *DEF* values decreased due to photon fluence reduction. When the mesh was close to the heart (position 1) or vertebral column (positions 4 and 5), the *DEF* surpassed 1.

In a nutshell, the *DEF* correlated directly with lung *Pt concentration* and inversely with depth. Conventional systemic Pt-based CT concurrent with permanent implant BT does not significantly change the lung *absorbed dose*, whereas unconventional Pt-based CT may lead to >2% dose increase in cases, where *Pt concentration* exceeds 0.2 mg/g lung tissue. In this case, the *absorbed dose* of healthy thoracic organs is reduced.

CONCLUSION

The results of this study show that the concurrent chemo-BT with conventional systemic Pt-based drugs, could not significantly change the lung absorbed dose while using the unconventional CT (multinuclear Pt-based CT drugs/regional CT), would lead to >2% dose changes when the Pt concentration exceeds 0.2 mg/g lung tissue. In the latter case, the absorbed dose of healthy thoracic tissues is also reduced. As clinical evaluations are not included in this simulation study, more complementary studies are required based on patients' dataset for lung concurrent chemo-BT.

Ethical approval

This research does not contain any study with human participants or animals performed by any of the authors. The other ethical issues have been taken into consideration.

Acknowledgements

The authors would like to thank vice chancellery for research and technology affairs of Shiraz University of Medical Sciences (SUMS) for supporting this research.

Financial support and sponsorship

Nil.

Conflicts of interest

There are no conflicts of interest.

REFERENCES

1. Jemal A, Siegel R, Ward E, Murray T, Xu J, Thun MJ. Cancer statistics, 2007. CA: A Cancer J Clin 2007;57:43-66.
2. Giaccone G. Systemic Treatment of Non-Small Cell Lung Cancer. Oxford: OUP; 2012. p. 2.
3. Devlin PM. Brachytherapy: Applications and Techniques. Philadelphia: Lippincott Williams & Wilkins; 2007. p. 142.
4. Mountain CF. Revisions in the international system for staging lung cancer. Chest 1997;111:1710-7.
5. Voynov G, Heron DE, Lin CJ, Burton S, Chen A, Quinn A, *et al*. Intraoperative 125 I Vicryl mesh brachytherapy after sublobar resection for high-risk stage I nonsmall cell lung cancer. Brachytherapy 2005;4:278-85.
6. Sutherland J, Furutani K, Thomson R. Monte Carlo calculated doses to treatment volumes and organs at risk for permanent implant lung brachytherapy. Phys Med Biol 2013;58:7061.
7. Sutherland J, Furutani K, Garces YI, Thomson R. Model-based dose calculations for 125I lung brachytherapy. Med Phys 2012;39:4365-77.
8. Sutherland J, Miksys N, Furutani K, Thomson R. Metallic artifact mitigation and organ-constrained tissue assignment for Monte Carlo calculations of permanent implant lung brachytherapy. Med Phys 2014;41:011712. doi: 10.1118/1.4851555.
9. Santos R, Colonias A, Parda D, Trombetta M, Maley RH, Macherey R, *et al*. Comparison between sublobar resection and 125 iodine brachytherapy after sublobar resection in high-risk patients with stage I non–small-cell lung cancer. Surgery 2003;134:691-7.
10. Peters S, Besse B. New Therapeutic Strategies in Lung Cancers. Springer International Publishing; 2014. p. 49.
11. Kernstine KH, Reckamp KL, Thomas CR. Lung Cancer: A Multidisciplinary Approach to Diagnosis and Management. Springer Publishing Company; 2010. p. xci-ii
12. Butts CA, Ding K, Seymour L, Twumasi-Ankrah P, Graham B, Gandara D, *et al*. Randomized phase III trial of vinorelbine plus cisplatin compared with observation in completely resected stage IB and II non–small-cell lung cancer: Updated survival analysis of JBR-10. J Clin Oncol 2009;28:29-34.
13. Van Dyk J, Keane T, Kan S, Rider W, Fryer C. Radiation pneumonitis following large single dose irradiation: A re-evaluation based on absolute dose to lung. Int J Radiat Oncol Biol Phys 1981;7:461-7.
14. Stewart DJ, Benjamin RS, Luna M, Feun L, Caprioli R, Seifert W, *et al*. Human tissue distribution of platinum after cis-diamminedichloroplatinum. Cancer Chemother Pharmacol 1982;10:51-4.
15. Kim ES, Lee JJ, He G, Chow C-W, Fujimoto J, Kalhor N, *et al*. Tissue platinum concentration and tumor response in non–small-cell lung cancer. J Clin Oncol 2012;30:3345-52.
16. Mostaghimi H, Mehdizadeh AR, Jahanbakhsh M, Dehghanian AR, Askari R. Quantitative determination of tumor platinum concentration of patients with advanced Breast, lung, prostate, or colorectal cancers undergone platinum-based chemotherapy. J Cancer Res Ther 2017;13:930-5.
17. Van Schil P. Lung Metastases and Isolated Lung Perfusion. New York: Nova Science Publishers; 2007. p. 205.
18. Zhukova O, Dobrynin I. Current results and perspectives of the use of human tumor cell lines for antitumor drug screening. Vopr Onkol 2001;47:706-9.
19. Pratesi G, Perego P, Polizzi D, Righetti S, Supino R, Caserini C, *et al*. A novel charged trinuclear platinum complex effective against cisplatin-resistant tumours: Hypersensitivity of p53-mutant human tumour xenografts. Br J Cancer 1999;80:1912-9.
20. Gatti L, Supino R, Perego P, Pavesi R, Caserini C, Carenini N, *et al*.

Apoptosis and growth arrest induced by platinum compounds in U2-OS cells reflect a specific DNA damage recognition associated with a different p53-mediated response. Cell Death Differentiation 2002;9:1352.
21. Zehnulova J, Kasparkova J, Farrell N, Brabec V. Conformation, recognition by high mobility group domain proteins, and nucleotide excision repair of DNA intrastrand cross-links of novel antitumor trinuclear platinum complex BBR3464. J Biol Chem 2001;276:22191-9.
22. Kasparkova J, Zehnulova J, Farrell N, Brabec V. DNA interstrand cross-links of the novel antitumor trinuclear platinum complex BBR3464 conformation, recognition by high mobility group domain proteins, and nucleotide excision repair. J Biol Chem 2002;277:48076-86.
23. Brabec V, Kasparkova J. Molecular aspects of resistance to antitumor platinum drugs. Drug Resist Updat 2002;5:147-61.
24. Kasparkova J, Pospisilova S, Brabec V. Different recognition of DNA modified by antitumor cisplatin and its clinically ineffective trans isomer by tumor suppressor protein p53. J Biol Chem 2001;276:16064-9.
25. Manzotti C, Pratesi G, Menta E, Di Domenico R, Cavalletti E, Fiebig HH, *et al*. BBR 3464: A novel triplatinum complex, exhibiting a preclinical profile of antitumor efficacy different from cisplatin. Clin Cancer Res 2000;6:2626-34.
26. Perego P, Caserini C, Gatti L, Carenini N, Romanelli S, Supino R, *et al*. A novel trinuclear platinum complex overcomes cisplatin resistance in an osteosarcoma cell system. Mol Pharmacol 1999;55:528-34.
27. Perego P, Gatti L, Caserini C, Supino R, Colangelo D, Leone R, *et al*. The cellular basis of the efficacy of the trinuclear platinum complex BBR 3464 against cisplatin-resistant cells. J Inorg Biochem 1999;77:59-64.
28. Choudhary MI. Frontiers in Anti-Cancer Drug Discovery. Vol 4. Sharjah: Bentham Science Publishers Incorporated; 2014. p. 317-8.
29. Mishra AK. Nanomedicine for Drug Delivery and Therapeutics. New York: John Wiley & Sons; 2013. p. 449.
30. Plummer R, Wilson R, Calvert H, Boddy A, Griffin M, Sludden J, *et al*. A phase I clinical study of cisplatin-incorporated polymeric micelles (NC-6004) in patients with solid tumours. Br J Cancer 2011;104:593-8.
31. Mansour HM, Rhee Y-S, Wu X. Nanomedicine in pulmonary delivery. Int J Nanomed 2009;4:299-319.
32. Müller H, Guadagni S. Regional chemotherapy for carcinoma of the lung. Surgical Oncol Clin North America 2008;17:895-917.
33. Osaki T, Hanagiri T, Nakanishi R, Yoshino I, Taga S, Yasumoto K. Bronchial arterial infusion is an effective therapeutic modality for centrally located early-stage lung cancer: Results of a pilot study. Chest 1999;115:1424-8.
34. Zarogoulidis P, Chatzaki E, Porpodis K, Domvri K, Hohenforst-Schmidt W, Goldberg EP, *et al*. Inhaled chemotherapy in lung cancer: Future concept of nanomedicine. Int J Nanomed 2012;7:1551-72.
35. Müller H. Combined regional and systemic chemotherapy for advanced and inoperable non-small cell lung cancer. Eur J Surg Oncol 2002;28:165-71.
36. Zhao G, Huang Y, Ye L, Duan L, Zhou Y, Yang K, *et al*. Therapeutic efficacy of traditional vein chemotherapy and bronchial arterial infusion combining with CIKs on III stage non-small cell lung cancer. Zhongguo Fei Ai Za Zhi 2009;12:1000-4.
37. Cypel M, Keshavjee S. Isolated lung perfusion. Front Biosci 2012;4:2226-32.
38. Tanaka T, Kaneda Y, Li T-S, Matsuoka T, Zempo N, Esato K. Digitonin enhances the antitumor effect of cisplatin during isolated lung perfusion. Ann Thorac Surg 2001;72:1173-8.
39. Ratto G, Toma S, Civalleri D, Passerone G, Esposito M, Zaccheo D, *et al*. Isolated lung perfusion with platinum in the treatment of pulmonary metastases from soft tissue sarcomas. J Thorac Cardiovasc Surg 1996;112:614-22.
40. Rudek MA, Chau CH, Figg W, McLeod HL. Handbook of Anticancer Pharmacokinetics and Pharmacodynamics. New York: Springer; 2014. p. 503.
41. Schröder C, Fisher S, Pieck AC, Müller A, Jaehde U, Kirchner H, *et al*. Technique and results of hyperthermic (41 degrees C) isolated lung perfusion with high-doses of cisplatin for the treatment of surgically relapsing or unresectable lung sarcoma metastasis. Eur J Cardiothorac Surg 2002;22:41-6.
42. Mostaghimi H, Mehdizadeh AR, Darvish L, Akbari S, Rezaei H. Mathematical formulation of 125 I seed dosimetry parameters and heterogeneity correction in lung permanent implant brachytherapy. J Cancer Res Ther 2017;13:436-41.
43. Rezaei H, Mostaghimi H, Mehdizadeh A. Modification of source strength in low-dose-rate lung brachytherapy with 125I and 103Pd seeds. J Biomed Phys Eng 2017;7:191-204.
44. Chen A, Galloway M, Landreneau R, d'Amato T, Colonias A, Karlovits S, *et al*. Intraoperative 125 I brachytherapy for high-risk stage I non-small cell lung carcinoma. Int J Radiat Oncol Biol Phys 1999;44:1057-63.
45. Johnson M, Colonias A, Parda D, Trombetta M, Gayou O, Reitz B, *et al*. Dosimetric and technical aspects of intraoperative I-125 brachytherapy for stage I non-small cell lung cancer. Phys Med Biol 2007;52:1237-45.
46. Sutherland JG. Monte Carlo Dose Calculations for Breast and Lung Permanent Implant Brachytherapy. Carleton University Ottawa; 2013. p. 15.
47. Taylor R, Yegin G, Rogers D. Benchmarking BrachyDose: Voxel based EGSnrc Monte Carlo calculations of TG-43 dosimetry parameters. Med Phys 2007;34:445-57.
48. White D, Woodard H, Hammond S. Average soft-tissue and bone models for use in radiation dosimetry. Br J Radiol 1987;60:907-13.
49. Rivard MJ, Coursey BM, DeWerd LA, Hanson WF, Saiful Huq M, Ibbott GS, *et al*. Update of AAPM Task Group No. 43 Report: A revised AAPM protocol for brachytherapy dose calculations. Med Phys 2004;31:633-74.
50. Rezaei H, Zabihzadeh M, Ghorbani M, Ahmadabad FG, Mostaghimi H. Evaluation of dose enhancement in presence of gold nanoparticles in eye brachytherapy by 103Pd source. Australas Phys Eng Sci Med 2017;40:545-53.